DOI: 10.1021/ic901906h

Inorganic Chemistry
Article

Reactivity of CuI and CuBr toward Et_2S: a Reinvestigation on the Self-Assembly of Luminescent Copper(I) Coordination Polymers

Michael Knorr,*,† Abdoulaye Pam,† Abderrahim Khatyr,† Carsten Strohmann,‡ Marek M. Kubicki,*,§ Yoann Rousselin,§ Shawkat M. Aly,⊥ Daniel Fortin,⊥ and Pierre D. Harvey*,⊥

†*Institut UTINAM, UMR CNRS 6213, Université de Franche-Comté, 25030 Besançon, France,* ‡*Anorganische Chemie, Technische Universität Dortmund, Otto-Hahn Strasse 6, D-97074 Dortmund, Germany,* §*Institut de Chimie Moléculaire, UMR CNRS 5260, Université de Bourgogne, F-21078 Dijon, France, and* ⊥*Département de Chimie, Université de Sherbrooke, Sherbrooke, Quebec, Canada J1K 2R*

Received September 30, 2009

CuI reacts with SEt_2 in hexane to afford the known strongly luminescent 1D coordination polymer $[(Et_2S)_3\{Cu_4(\mu_3\text{-}I)_4\}]_n$ (**1**). Its X-ray structure has been redetermined at 115, 235, and 275 K in order to address the behavior of the cluster-centered emission and is built upon $Cu_4(\mu_3\text{-}I)_4$ cubane-like clusters as secondary building units (SBUs), which are interconnected via bridging SEt_2 ligands. However, we could not reproduce the preparation of a coordination polymer with composition $[(Et_2S)_3\{Cu_4(\mu_3\text{-}Br)_4\}]_n$ as reported in *Inorg. Chem.* **1975**, *14*, 1667. In contrast, the autoassembly reaction of SEt_2 with CuBr results in the formation of a novel 1D coordination polymer of composition $[(Cu_3Br_3)(SEt_2)_3]_n$ (**2**). The crystal structure of **2** has been solved at 115, 173, 195, and 235 K. The framework of the luminescent compound **2** consists of a corrugated array with alternating $Cu(\mu_2\text{-}Br)_2Cu$ rhomboids, which are connected through two bridging SEt_2 ligands to a tetranuclear open-cubane Cu_4Br_4 SBU, ligated on two external Cu atoms with one terminal SEt_2. The solid-state luminescence spectra of **1** and **2** exhibit intense halide-to-metal charge-transfer emissions centered at 565 and 550 nm, respectively, at 298 K. A correlation was also noted between the change in the full width at half-maximum of the emission band between 298 and 77 K and the relative flexibility of the bridging ligand. The emission properties of these materials are also rationalized by means of density functional theory (DFT) and time-dependent DFT calculations performed on **1**.

Introduction

Since the early 1970s, it has been well-known that the reaction of copper(I) halides with monodentate aliphatic and aromatic N donors led sometimes, depending on the reaction conditions, to both discrete molecular CuX·L adducts or the formation of polymeric networks.[1] For instance, the reaction of CuI with MeCN in the presence of the crown ether dibenzo-18-crown-6 affords the tetranuclear cluster $[(MeCN)_4\{Cu_4(\mu_3\text{-}I)_4\}]\cdot$dibenzo-18-crown-6, whereas in the absence of the crown ether, the ribbonlike polymer $[CuI(MeCN)]_n$ is produced.[2] The treatment of CuI with pyridine and its derivatives leads to either the molecular cubane-like cluster $[(py)_4\{Cu_4(\mu_3\text{-}I)_4\}]$ or the 1D coordination polymer $[CuI(py)]_n$.[3−5] In the case of the polymeric $[CuI(4\text{-picoline})]_n$, exposure of the solid to toluene vapor induces a transformation to the molecular cluster $[(4\text{-picoline})_4\{Cu_4(\mu_3\text{-}I)_4\}]\cdot 2$toluene.[6] More recent works have demonstrated that the reaction of CuX with bisdentate (ditopic) or polydentate N-donor ligands may generate macrocycles[7] and even 2D and 3D metallorganic frameworks, which incorporate the closed cubane-like Cu_4X_4 motif as a secondary building unit (SBU).[8−11] Parallel with the crystallographic characterization, the often intense luminescence properties of these Cu_4X_4-containing materials intrigued several research

*To whom correspondence should be addressed. E-mail: michael.knorr@univ-fcomte.fr (M.K.), marek.kubicki@u-bourgogne.fr (M.M.K.), Pierre.Harvey@USherbrooke.ca (P.D.H.).

(1) (a) Malik, A. U. *J. Inorg. Nucl. Chem.* **1967**, *29*, 2106–2107. (b) Hardt, H. D.; de Ahna, H. D. *Z. Naturwiss.* **1970**, *57*, 244–245. (c) Schramm, V.; Fischer, K. F. *Naturwissenschaften* **1974**, *67*, 500–501. (d) Schramm, V. *Inorg. Chem.* **1978**, *17*, 714–1718. (e) For a review, see: Caulton, K. G.; Davies, G.; Holt, E. M. *Polyhedron* **1990**, *19*, 2319–2351.

(2) (a) Jasinski, J. P.; Rath, N. P.; Holt, E. M. *Inorg. Chim. Acta* **1985**, *97*, 91–97. (b) Healy, P. C.; Kildea, J. D.; Skelton, B. W.; White, A. H. *Aust. J. Chem.* **1989**, *42*, 79–91.

(3) Raston, C. L.; White, A. H. *J. Chem. Soc., Dalton Trans.* **1976**, 2153–2156.

(4) (a) Eitel, E.; Oelkrug, D.; Hiller, W.; Straehle, J. *Z. Naturforsch.* **1980**, *35B*, 1247–1253. (b) Radjaipour, M.; Oelkrug, D. *Ber. Bunsen-Ges.* **1978**, *82*, 159–163.

(5) Schramm, V. *Cryst. Struct. Commun.* **1982**, *11*, 1549–1556.

(6) Cariati, E.; Bu, X.; Ford, P. C. *Chem. Mater.* **2000**, *12*, 3385–3391.

(7) Wang, R.-H.; Hong, M.-C.; Jun-Hua Luo, R. C.; Weng, J.-B. *Eur. J. Inorg. Chem.* **2002**, 3097–3100.

(8) Hu, S.; Tong, M.-L. *Dalton Trans.* **2005**, 1165–1167.

(9) Wang, G.-X.; Xiong, R.-G. *Chin. J. Chem.* **2007**, *25*, 1405–1408.

(10) Zhou, H.; Lin, P.; Li, Z.-H.; Du, S.-W. *J. Mol. Struct.* **2008**, *881*, 21–27.

(11) Li, T.; Du, S.-W. *J. Cluster Sci.* **2008**, *19*, 323–330.

 Published on Web 05/28/2010

groups, whom investigated both experimentally and theoretically their photophysics.[4,12−14] Noteworthy is the pioneering work of Hardt et al., who found that the emission spectra are, in some cases, temperature-dependent. They coined the term "luminescence thermochromism" for this reversible phenomenon.[15] Following the progress of computational methods, extended Hückel, ab initio, density functional theory (DFT), and recently time-dependent DFT (TDDFT) calculations have been performed to provide a theoretical understanding of the Cu···Cu interaction and of the photophysical properties of the $[Cu_4X_4L_4]$ systems.[16−19] It is now established that the low-energy emission results from a triplet-cluster excited state (^{3}CC*), which presents a profound deformation of the cluster core geometry (increase of the Cu−I distances associated with the shortening of the Cu···Cu separations) compared to the ground state. Concerning the high-energy transition, a triplet-state halide-to-metal charge transfer (^{3}X-MCT) is involved.[20]

Like N, P, and As donors, also group 16 ligands of the soft elements S, Se, and Te (according to the hard and soft acids and bases principle) easily form stable adducts with copper(I) halides. The interactions of mono- and polydentate thioethers with CuX may lead to discrete mono- or dinuclear species or afford in a self-assembly process polynuclear complexes, which display a fascinating diversity of stoichiometries and geometries.[21−23] The most common motifs are the infinite I−Cu−I−Cu−I zigzag chains, ladderlike CuI ribbons, iodide-bridged rhomboid dimers, and tetranuclear cubane-like Cu_4I_4 clusters (Scheme 1).

In the context of our research interest on the coordination chemistry of dithioether ligands,[24] we recently reported the

Scheme 1. Representations of Some Common CuX·L Motifs[a]

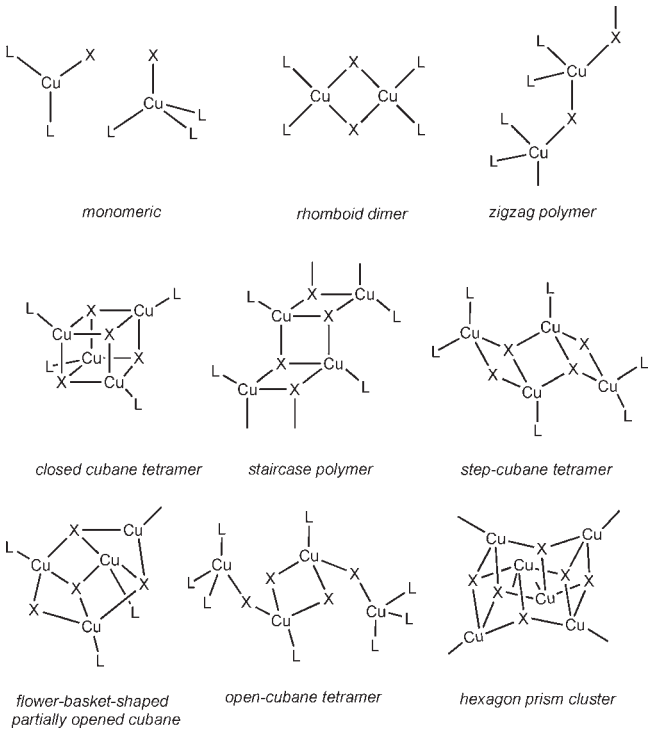

[a] The di- and polynuclear cluster units may be assembled by additional Cu···Cu interactions if *d*(Cu···Cu) is close or below the sum of the van der Waals radii (2.8 Å) of two Cu atoms.

influence of the spacer length of dithioether ligands on the solid-state structures of CuI-based coordination polymers. With bis(phenylthio)methane, a 1D necklace-like chain with a composition of $[Cu_4I_4\{\mu\text{-PhSCH}_2\text{SPh}\}_2]_n$ was obtained, whereas the reaction with $PhS(CH_2)_2SPh$ resulted in the formation of a 2D coordination polymer $[(CuI)_2\{\mu\text{-PhS}(CH_2)_2\text{SPh}\}_2]_n$, built upon dimeric Cu_2I_2 units.[25a] With the flexible ligand $PhS(CH_2)_4SPh$, an interpenetrated 2D coordination polymer with a composition of $[Cu_4I_4\{\mu\text{-PhS}_2(CH_2)_4\text{SPh}\}_2]_n$ was generated. In the case of the more rigid ligand $PhSCH_2C{\equiv}CCH_2SPh$, the formation of a 3D network incorporating a Cu_6I_6 hexagon prism cluster as the SBU has been crystallographically established (Scheme 1).[25b] Because the photophysics of these strongly luminescent species are very interesting, we were intrigued to extend our experimental and theoretical investigations to other related CuI·thioether systems.[25c] A promising candidate for the comparative photophyscical studies seemed to be the easy to synthesize polymer $[(Et_2S)_3\{Cu_4(\mu_3\text{-I})_4\}]_n$ (**1**), which had been prepared and structurally characterized more than 30 years ago by Potenza et al.[26,27a] We report herein on a more accurate redetermination of the crystal structure of this

(12) For a recent review on luminescent copper compounds, see: Armaroli, N.; Accorsi, G.; Cardinali, F.; Listorti, A. *Top. Curr. Chem.* **2007**, *280*, 69–115.
(13) (a) Ford, P. C.; Vogler, A. *Acc. Chem. Res.* **1993**, *26*, 220–226. (b) Ford, P. C. *Coord. Chem. Rev.* **1994**, *132*, 129–140. (c) Ford, P. C.; Cariati, E.; Bourassa, J. *Chem. Rev.* **1999**, *99*, 3625–3648.
(14) Tard, C.; Perruchas, S.; Maron, S.; Le Goff, X. F.; Guillen, F.; Garcia, A.; Vigneron, J.; Etcheberry, A.; Gacoin, T.; Boilot, J.-P. *Chem. Mater.* **2008**, *20*, 7010–7016.
(15) (a) Ahna, H. D. D.; Hardt, H. D. *Z. Anorg. Allg. Chem.* **1972**, *387*, 61–71. (b) Hardt, H. D.; Pierre, A. *Z. Anorg. Allg. Chem.* **1973**, *402*, 107–112. (c) Hardt, H. D.; Pierre, A. *Inorg. Chim. Acta* **1977**, *25*, L59–L60.
(16) Hu, G.; Mains, G. J.; Holt, E. M. *Inorg. Chim. Acta* **1995**, *240*, 559–565.
(17) (a) Mehrotra, P. K.; Hoffmann, R. *Inorg. Chem.* **1978**, *17*, 2187–2189. (b) Vega, A.; Saillard, J.-Y. *Inorg. Chem.* **2004**, *43*, 4012–4018.
(18) Carvajal, M. A.; Alvarez, S.; Novoa, J. J. *Chem.—Eur. J.* **2004**, *10*, 2117–2132.
(19) Fernández, E. J.; Laguna, A.; López-de-Luzuriaga, J. M.; Monge, M.; Montiel, M.; Olmos, M. E.; Rodríguez-Castillo, M. *Organometallics* **2006**, *25*, 3639–3646.
(20) Angelis, F. D.; Fantacci, S.; Sgamellotti, A.; Cariati, E.; Ugo, R.; Ford, P. C. *Inorg. Chem.* **2006**, *45*, 10576–10584.
(21) (a) Munakata, M.; Kuroda-Sowa, T.; Maekawa, M.; Honda, A.; Kitagawa, S. *J. Chem. Soc., Dalton Trans.* **1994**, 2771–2775. (b) Adams, R. D.; Huang, M.; Johnson, S. *Polyhedron* **1998**, *17*, 2775–2780. (c) Peng, R.; Li, D. *Coord. Chem. Rev.* **2010**, *254*, 1–18.
(22) (a) Blake, A. J.; Brooks, N. R.; Champness, N. R.; Hanton, L. R.; Hubberstey, P.; Schröder, M. *Pure Appl. Chem.* **1998**, *70*, 2351–2357. (b) Brooks, N. R.; Blake, A. J.; Champness, N. R.; Cooke, P. A.; Hubberstey, P.; Proserpio, D. M.; Wilson, C.; Schröder, M. *J. Chem. Soc., Dalton Trans.* **2001**, 456–465.
(23) (a) Heller, M.; Sheldrick, W. S. *Z. Anorg. Allg. Chem.* **2003**, *629*, 1589–1595. (b) Heller, M.; Sheldrick, W. S. *Z. Anorg. Allg. Chem.* **2004**, *630*, 1869–1874.
(24) (a) Knorr, M.; Guyon, F.; Jourdain, I.; Kneifel, S.; Frenzel, J.; Strohmann, C. *Inorg. Chim. Acta* **2003**, *350*, 455–466. (b) Knorr, M.; Peindy, H. N.; Guyon, F.; Sachdev, H.; Strohmann, C. *Z. Anorg. Allg. Chem.* **2004**, *630*, 1955–1961. (c) Peindy, H. N.; Guyon, F.; Knorr, M.; Strohmann, C. *Z. Anorg. Allg. Chem.* **2005**, *631*, 2397–2400. (d) Peindy, H. N.; Guyon, F.; Jourdain, I.; Knorr, M.; Schildbach, D.; Strohmann, C. *Organometallics* **2006**, *25*, 1472–1479. (e) Clément, S.; Guyard, L.; Knorr, M.; Villafane, F.; Strohmann, C.; Kubicki, M. M. *Eur. J. Inorg. Chem.* **2007**, 5052–5061.
(25) (a) Peindy, H. N.; Guyon, F.; Khatyr, A.; Knorr, M.; Strohmann, C. *Eur. J. Inorg. Chem.* **2007**, 1823–1828. (b) Knorr, M.; Guyon, F.; Khatyr, A.; Däschlein, C.; Strohmann, C.; Aly, S. M.; Abd-El-Aziz, A. S.; Fortin, D.; Harvey, P. D. *Dalton Trans.* **2009**, 948–955. (c) Harvey, P. D.; Knorr, M. *Macromol. Rapid Commun.* **2010**, *31*, 808−826.
(26) San Filippo, J.; Zyontz, L. E.; Potenza, J. *Inorg. Chem.* **1975**, *14*, 1667–1671.
(27) (a) Compound **1** has been the object of an IR and Raman spectroscopic study: Bowmaker, G. A.; Knappstein, R. J.; Tham, S. F. *Aust. J. Chem.* **1978**, *31*, 2137–2143. (b) In contrast to polymeric 1, $[(dodecylSMe)_4\{Cu_4(\mu_3\text{-I})_4\}]$ is reported to be monomeric with Cu−Cu distances in the range 266.9−284.6 pm at 299 K: Paulson, H.; Berggrund, M.; Fischer, A.; Kloo, L. *Z. Anorg. Allg. Chem.* **2004**, *630*, 413–416.

1D polymer incorporating tetranuclear cubane-like Cu_4I_4 cluster units as SBUs and the photophysics at different temperatures as well on the electronic structure of this luminescent compound. Furthermore, we prepared for comparison purposes the corresponding $CuBr \cdot SEt_2$ adduct (**2**), elucidated its hitherto unknown crystal structure displaying a quite unusual alternation of $Cu(\mu_2\text{-}Br)_2Cu$ rhomboids and tetranuclear open-cubane-like Cu_4Br_4 SBUs within the 1D chain, and analyzed the emission spectra of this compound.

Results and Discussion

1. Synthesis and Structural Description of Polymer $[(Et_2S)_3\{Cu_4(\mu_3\text{-}I)_4\}]_n$ (1). Cuprous halides are known to produce in some rare cases discrete mono- and dinuclear species upon treatment with a simple aliphatic thioether RSR. If CuCl is dissolved in neat SMe_2, the mononuclear adduct $CuCl(SMe_2)_3$ can be isolated after crystallization at low temperature.[28a] With the heterocyclic thioether compound tetrahydrothiophene (THT), the dinuclear complex $[(THT)_2Cu(\mu_2\text{-}I)_2Cu(THT)_2]$ is formed.[28b,29] However, depending on the reaction conditions, copper halides seem to prefer to form polymeric networks with a variety of aliphatic thioethers RSR. Bridging halide ligands, in general, assemble these networks. Furthermore, and in contrast to monodentate N and P donors, the presence of two nonbonding doublets on the S-donor atom allows also a bridging $\mu_2\text{-}SR_2$ bonding mode. The first report on the rational construction of Cu^I coordination polymers of this type stems from Potenza et al., who reacted CuX with neat Me_2S, Et_2S, Pr_2S, and Bu_2S.[26] Whereas Me_2S reacts with CuX to give 1:1 complexes, a similar reaction with Et_2S was reported to produce a homologous series of complexes with a ligand-to-Cu ratio of 3:4. As stated in the Introduction, this unusual stoichiometry was structurally established for the polymeric $Et_2S \cdot CuI$ adduct **1**. Later work from van Koten et al. established that the structure of the 1:1 $CuBr \cdot SMe_2$ adduct consists of a layered polymeric 2D network with composition $[(\mu\text{-}Me_2S)_2\{Cu_2(\mu_2\text{-}Br)_2\}]_n$.[30]

In the context of our interest in the luminescence properties of $CuX \cdot$dithioether compounds, we were intrigued by the photophysics of polymer **1** ligated by simple aliphatic RSR donors and compared the data with those of $CuI \cdot ArS(CH_2)_nSAr$ ($n = 1-8$) adducts (unpublished). Because the quality of the reported structure of **1** is poor with high estimated standard deviations and without H atoms,[26] we decided to redetermine its crystal structure. Single crystals suitable for X-ray analysis were obtained by recrystallization of **1** from a concentrated MeCN solution at 5 °C. In order to obtain the structural information related to temperature-dependent photophysical data (see below, and, in particular, to luminescence thermochromism), we carried out X-ray measurements on the same crystal at variable temperature. For practical reasons (silicon grease as glue), the limiting temperatures are 115 and 275 K, with an intermediate one chosen at 235 K. The overall structure of **1** is the same as that reported by Potenza et al.[26,27b]

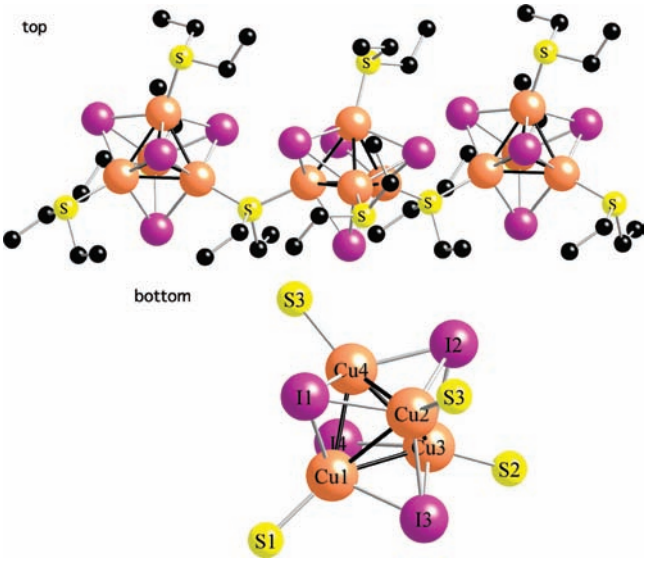

Figure 1. (top) View of the Et_2S-bridged 1D ribbon of **1** along the *a* axis (115 K). The H atoms are omitted for clarity (an ORTEP plot is depicted in Figure S1 in the Supporting Information). (bottom) Cu_4I_4 core of **1** with the numbering scheme.

The highly distorted (small Cu_4 and large I_4 tetrahedra) cubane-like Cu_4I_4 units bearing two terminal SEt_2 (S1 and S2) are bridged with the third SEt_2 ligand S3 (Figures 1 and S1 in the Supporting Information), hence leading to the 1D chains running parallel to the *a* unit cell axis and zigzagging in a plane parallel to *ab* (Figure S2 in the Supporting Information). There are two chains crossing the unit cell, each of them containing two Cu_4I_4 SBUs inside this unit cell. The individual chains are separated with infinite planar zones formed by interpenetrating terminal ethyl groups of the SEt_2 ligands based on the S1 atom in the *b*(*a*) in-plane direction and on the S2 atom in the *z*(*a*) in-plane one. The unit cell dilates from 2615 $Å^3$ (115 K) to 2704 $Å^3$ (275 K) (3.4%), with the greatest increase of *b* [11.2959(3)−11.5203(3) Å; Δ of 0.23 Å] and *c* [18.1129(5)−18.3708(6) Å; Δ of 0.26 Å] unit cell parameters and with the much smaller increase of *a* [13.1104(4)−13.1590(4) Å; Δ of 0.05 Å] (Table 1). The crystal data, data collection, and structure refinement of **1** and **2** are given in Table 1.

Evolution of the Cu−S and Cu−I bond lengths as a function of the temperature is not regular and varies for mean values at 115, 235, and 275 K as follows (in Å): Cu−S(terminal), 2.306(1), 2.304(2), and 2.295(3); Cu−S(bridging), 2.333(1), 2.336(2), and 2.331(2); Cu−I, 2.6828(7), 2.6863(9), and 2.6854(11). On the other hand, the Cu···Cu distances within the Cu_4I_4 units (Table 2), which are expected to play an important role in their photophysical properties, increase almost monotonically with increasing temperature. The mean values equal 2.7562(9), 2.7835(12), and 2.7944(14) Å and vary by about 0.04 Å over the 160 K range. The largest variation concerns the Cu1···Cu4 distance (second longest, difference ~0.05 Å), which is roughly oriented toward the *bc* crystal diagonal direction, where the largest dilation of the unit cell is observed, whereas the smallest one is observed for Cu1···Cu2 (first longest, 0.025 Å). The Cu1 atom bears the terminal SEt_2 (S1 atom), while the Cu2 and Cu4 atoms are coordinated with the bridging SEt_2 ligands (S3 atoms).

(28) (a) Olbrich, F.; Maelger, H.; Klar, G. *Transition Met. Chem.* **1992**, *17*, 525–529. (b) Maelger, H.; Olbrich, F.; Kopf, J.; Abeln, D.; Weiss, E. *Z. Naturforsch.* **1992**, *47B*, 12–17. In this reference, also the structure of the 1D polymer $[(Cu_2Br_2)(THT)_3]_n$, resulting from the reaction of CuBr with THT, is described.

(29) Noren, B.; Oskarsson, A. *Acta Chem. Scand.* **1987**, *A41*, 12–17.

(30) Lenders, B.; Grove, D. M.; van Koten, G.; Smeets, W. J. J.; Van der Sluis, P.; Spek, A. L. *Organometallics* **1991**, *10*, 786–791.

Table 1. Crystal Data, Data Collection, and Structure Refinement

	1−275 K	1−235 K	1−115 K	2−173 K	2−235 K	2−195 K	2−115 K
formula	$C_{12}H_{30}Cu_4I_4S_3$	$C_{12}H_{30}Cu_4I_4S_3$	$C_{12}H_{30}Cu_4I_4S_3$	$C_{12}H_{30}Br_3Cu_3S_3$	$C_{12}H_{30}Br_3Cu_3S_3$	$C_{12}H_{30}Br_3Cu_3S_3$	$C_{12}H_{30}Br_3Cu_3S_3$
fw	1032.37	1032.37	1032.37	700.89	700.89	700.89	700.89
temperature/K	275	235	115	173	235	195	115
wavelength/Å	0.710 73	0.710 73	0.710 73	0.710 73	0.710 73	0.710 73	0.710 73
cryst syst	monoclinic	monoclinic	monoclinic	orthorhombic	orthorhombic	orthorhombic	orthorhombic
space group	$P2_1/a$	$P2_1/a$	$P2_1/a$	*Pbcn*	*Pbcn*	*Pbcn*	*Pbcn*
a/Å	13.1590(4)	13.1469(4)	13.1104(4)	14.7789(17)	14.9267(3)	14.7918(4)	14.6750(5)
b/Å	11.5203(3)	11.4443(3)	11.2959(3)	12.9264(15)	12.8977(2)	12.9259(3)	12.9230(3)
c/Å	18.3708(6)	18.3143(6)	18.1129(5)	23.410(3)	23.5086(4)	23.4291(6)	23.3158(4)
β/deg	103.854(1)	103.420(1)	102.874(1)	90			
volume/Å^3	2703.92(14)	2680.28(14)	2614.98(13)	4472.2(9)	4525.88(14)	4479.6(2)	4421.5(2)
Z	4	4	4	8	8	8	8
density (calculated)/(g/cm^3)	2.536	2.558	2.622	2.082	2.057	2.079	2.106
abs coeff/mm^{-1}	7.899	7.968	8.167	8.460	8.360	8.446	8.556
F(000)	1912	1912	1912	2736	2736	2736	2736
cryst size/mm	0.2 × 0.2 × 0.12	0.2 × 0.2 × 0.12	0.2 × 0.2 × 0.12	0.40 × 0.20 × 0.20	0.22 × 0.20 × 0.12	0.22 × 0.20 × 0.12	0.22 × 0.20 × 0.12
θ range for data collection/deg	2.38−27.48	2.39−27.50	2.41−27.48	1.74−27.00	1.73−27.46	1.74−27.48	2.10−27.48
index ranges	$-17 \le h \le 17$, $-14 \le k \le 14$, $-23 \le l \le 23$	$-17 \le h \le 17$, $-14 \le k \le 14$, $-23 \le l \le 23$	$-16 \le h \le 17$, $-14 \le k \le 11$, $-23 \le l \le 23$	$-18 \le h \le 18$, $-16 \le k \le 16$, $-29 \le l \le 29$	$-19 \le k \le 17$, $-16 \le k \le 16$, $-30 \le l \le 28$	$-19 \le k \le 18$, $-16 \le k \le 16$, $-28 \le l \le 30$	$-19 \le k \le 18$, $-16 \le k \le 16$, $-30 \le l \le 30$
reflns collected	21 619	11 485	10 644	93 410	36 080	23 045	33 594
indep reflns	6168 [R(int) = 0.053]	6059 [R(int) = 0.028]	5906 [R(int) = 0.023]	4877 [R(int) = 0.0647]	5168 [R(int) = 0.0668]	5135 [R(int) = 0.0775]	5079 [R(int) = 0.0712]
refinement method	full-matrix least squares on F^2	full-matrix least squares on F^2	full-matrix least squares on F^2	full-matrix least squares on F^2	full-matrix least squares on F^2	full-matrix least squares on F^2	full-matrix least squares on F^2
data/restraints/param	6168/0/214	6059/0/214	5906/0/214	4877/0/196	5168/0/196	5135/0/196	5079/0/196
GOF on F^2	1.140	1.131	1.189	1.037	1.113	1.124	1.114
final R indices [$I > 2\sigma(I)$]	R1 = 0.0456, wR2 = 0.0938	R1 = 0.0376, wR2 = 0.0786	R1 = 0.0305, wR2 = 0.0661	R1 = 0.0241, wR2 = 0.0611	R1 = 0.0624, wR2 = 0.0828	R1 = 0.0802, wR2 = 0.1040	R1 = 0.0494, wR2 = 0.0741
R indices (all data)	R1 = 0.0597, wR2 = 0.1007	R1 = 0.0473, wR2 = 0.0836	R1 = 0.0366 wR2 = 0.0676	R1 = 0.0302 wR2 = 0.0652	R1 = 0.0409 wR2 = 0.0737	R1 = 0.0524 wR2 = 0.0929	R1 = 0.0370 wR2 = 0.0694
largest diff peak and hole/(e/Å^3)	1.002, −0.897	0.728, −0.916	1.096, −0.963	0.485, −0.744	0.727, −0.775	0.627, −0.895	0.751, −0.648

Table 2. Cu···Cu Distances (Å) in **1** Found at Different Temperatures

Cu···Cu	115 K	235 K	275 K
Cu1···Cu2	2.8641(9)	2.8812(12)	2.8902(14)
Cu1···Cu4	2.7596(9)	2.8000(12)	2.8135(14)
Cu3···Cu4	2.7544(9)	2.7795(11)	2.7872(14)
Cu2···Cu4	2.7413(9)	2.7681(11)	2.7819(13)
Cu1···Cu3	2.7410(9)	2.7655(12)	2.7762(16)
Cu2···Cu3	2.6767(9)	2.7064(12)	2.7172(14)
mean	2.7562	2.7835	2.7944

Thus, variation of the Cu···Cu distances in **1** does not depend on the bridging or terminal nature of the S atoms.

The mean Cu···Cu distances observed in **1** are longer than those in the luminescent polymer $[Cu_4I_4(SMe_2)_3]_n$ [2.6681(9)−2.7138(12) Å; mean 2.690(1) Å at 173 K][31] and in $[Cu_2I_2(SMe_2)_3]_n$ [2.684(1) Å].[28b] They are also longer, but only by 0.04 Å, than that in Kim's group complex $[Cu_4I_4\mathbf{L1}_2]_n$ [**L1** = 2-(cyclohexylthio)-1-thiomorpholinoethanone, bidentate dithioether ligand] solvated with CH_3CN and *n*-hexane and for which a variable-temperature X-ray study has been performed in the range of 123−298 K.[32] The mean Cu···Cu distances found therein are 2.7174(10) (123 K), 2.7403(13) (223 K), and 2.757(3) Å (298 K). Their overall difference within the 175 K range is 0.04 Å, like in the structure of **1**. The largest variation of Cu···Cu distances (0.05 Å) is related to the long Cu···Cu contact. This latter product exhibits no shift of the luminescence band maxima between 298 and 77 K. On the other hand, the crystallization solvent free form of Kim's polymer $[Cu_4I_4\mathbf{L1}_2]_n$ exhibits a 2D network with even shorter Cu···Cu distances of 2.7005(11) (123 K), 2.7131(18) (223 K), and 2.729(2) (298 K) Å, with an overall difference of 0.03 Å that is smaller than that observed in **1**. The largest variations of individual Cu···Cu distances (0.06 and 0.05 Å) in Kim's solvent-free compound are observed for the longest Cu···Cu contacts. Note that the longest Cu1···Cu2 distance in **1** undergoes the smallest variation of 0.025 Å, while the second longest (Table 2) Cu1····Cu4 distance reaches 0.05 Å on warming. It is worth noting that a large red shift of 60 nm of the emission band from 298 to 77 K is recorded for crystallization of the solvent-free form of $[Cu_4I_4\mathbf{L1}_2]_n$[32] and that the contraction of the unit cell volume therein is of only 2.2% versus 3.4% observed for **1**.

2. Synthesis and Structural Description of Polymer $[(Cu_3Br_3)(SEt)_3]_n$ (2). In their original work, Filippo and Potenza mixed CuBr with neat SEt_2 and recrystallized the crude product from a $MeCN/SEt_2$ mixture. On the basis of elemental analysis, they suggested that the resulting product is isostructural with **1**, i.e., having a composition of $[(Et_2S)_3\{Cu_4(\mu_3\text{-}Br)_4\}]_n$. Because the crystal structure of this $CuBr\cdot Et_2S$ adduct **2** has not yet been described, we dissolved CuBr in neat Et_2S. After the addition of heptane, single crystals grew, forming large colorless blocks. Their X-ray structure was determined on one crystal of 0.40 × 0.20 × 0.20 mm size at 173 K and on another sample of 0.22 × 0.20 × 0.12 mm at 115, 195, and 235 K. Surprisingly, the architecture of the resulting 1D network differs clearly from that of **1**. Indeed, it consists of centrosymmetric rhomboidal Cu dimers that are linked to a distorted open-stepped-cubane Cu_4Br_4 motif that exhibits a 2-fold axis symmetry. The connectivity between the dinuclear rhomboids and the tetranuclear open cubanes operates through the planar five-membered Cu3−S2−Cu1−Cu2−S3 rings. Thus, this arrangement gives rise to an infinite 1D chain (Figure 2; an ORTEP drawing for the 115 K structure is given in Figure S3 in the Supporting Information). The parallel arrangement of these undulating chains in the packing is shown at the bottom of Figure 2 and in Figure S4 in the Supporting Information. The Cu···Cu distances are gathered in Table 3.

Note also that there are two bridging (S2 and S3) and one terminal (S1) thioether ligands in **2**, whereas there are one bridging and two terminal thioether ligands in **1**. As in the structure of **1**, there is no regular variation of the Cu−Br and Cu−S bonds with temperature (see the CIF files). However, the terminal Cu1−S1 bond lengths are systematically shorter than the mean values of the bridging Cu1−S2, Cu2−S3, Cu3−S2, and Cu3−S3 ones at 115, 173, 195, and 235 K: 2.280(1) vs 2.325(1), 2.2783(8) vs 2.331(1), 2.278(1) vs 2.332(2), and 2.279(1) vs 2.335(2) Å, respectively. On the other hand, the Cu···Cu distances exhibit some curious evolution (Table 3). The shortest Cu1−Cu2 bond length in the open Cu_4Br_4 unit close to 2.73 Å increases upon warming by ∼0.04 Å (extrapolated over 160 K). The central Cu2···Cu2#1 distance therein evolves in a similar manner. Surprisingly, the Cu3···Cu3#2 nonbonding (or metallophilic bonding) separation in the rhomboidal dimer decreases upon warming. There is, however, an overall crystal dilation of 3.5−3.6% within the 160 K range, which is slightly higher than that observed for **1** (3.4%).

It is worth noting that the copper coordination polymers incorporating two different inorganic core motifs are very scarce.[33−36] The mode of alternation of two different $(CuBr)_n$ motifs, a dinuclear $Cu_2(\mu_2\text{-}Br)_2$ SBU and a tetranuclear Cu_4Br_4 SBU, encountered for the construction of this 1D coordination polymer is to our knowledge unique. The quite long Cu3···Cu3#2 contact close to 3.0 Å in the $Cu(\mu_2\text{-}Br)_2Cu$ rhomboid is somewhat longer than that reported for $[(\mu\text{-}Me_2S)_2\{Cu_2(\mu_2\text{-}Br)_2\}]_n$ [2.9512(6) Å],[30] corresponds to that of 2D polymer $[(tetrathiaphthalazinophane)_2\{Cu_2(\mu_2\text{-}Br)_2\}]_n$ [3.060(6) Å],[37] and deserves no further comment.[38] However, the $Cu_4Br_4S_4$ cluster (S = sulfur donor) in polymer **2** exhibits an unprecedented open-cubane SBU with two μ_2-Br and two μ_3-Br ligands. This novel motif is an intermediate version between the flower-basked-shaped partially

(31) Zhou, J.; Bian, G.-Q.; Dai, J.; Zhang, Y.; Zhu, Q.-Y.; Lu, W. *Inorg. Chem.* **2006**, *45*, 8486–8488.
(32) Kim, T. H.; Shin, Y. W.; Jung, J. H.; Kim, J. S.; Kim, J. *Angew. Chem., Int. Ed.* **2008**, *47*, 685–688.
(33) Kanehama, R.; Umemiya, M.; Iwahori, F.; Miyasaka, H.; Sugiura, K.-I.; Yamashita, M.; Yokochi, Y.; Ito, H.; Kuroda, S.-I.; Kishida, H.; Okamoto, H. *Inorg. Chem.* **2003**, *42*, 7173–7181.
(34) Wang, J.; Zheng, S.-L.; Hu, S.; Zhang, Y.-H.; Tong, M.-L. *Inorg. Chem.* **2007**, *46*, 795–800.
(35) Lee, J. Y.; Lee, S. Y.; Sim, W.; Park, K.-M.; Kim, J.; Lee, S. S. *J. Am. Chem. Soc.* **2008**, *130*, 6902–6903.
(36) Huang, X.-F.; Fu, D.-W.; Xiong, R.-G. *Cryst. Growth Des.* **2008**, *8*, 1795–1797.
(37) Chen, L.; Thompson, L. K.; Tandon, S. S.; Bridson, J. N. *Inorg. Chem.* **1993**, *32*, 4063–4068.
(38) For other examples of thioether polymers incorporating $Cu_2(\mu_2\text{-}Br)_2$ SBUs, see: (a) Barnes, J. C.; Paton, J. D. *Acta Crystallogr.* **1982**, *B38*, 3091–3093. (b) Munakata, M.; Wu, L. P.; Kuroda-Sowa, T.; Maekawa, M.; Suenaga, Y.; Nakagawa, S. *J. Chem. Soc., Dalton Trans.* **1996**, 1525–1530. (c) Lucas, C. R.; Liu, S. *Can. J. Chem.* **1996**, *74*, 2340–2348. (d) Yim, H. W.; Tran, L. M.; Pullen, E. E.; Rabinovich, D.; Liable-Sands, L. M.; Concolino, T. E.; Rheingold, A. L. *Inorg. Chem.* **1999**, *38*, 6234–6239.

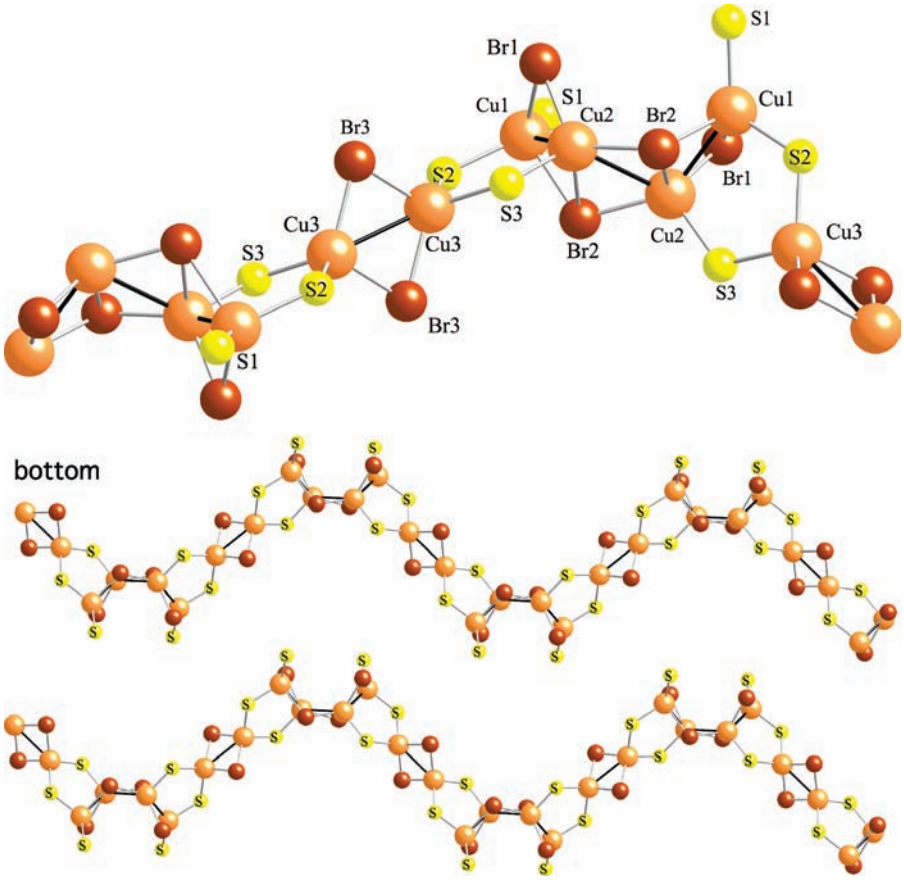

Figure 2. (top) View of the Et_2S-bridged 1D chain of **2** incorporating alternating dinuclear $Cu_2(\mu\text{-}Br)_2$ and tetranuclear $Cu_4(\mu\text{-}Br)_4$ motifs along the *c* axis. The ethyl groups are omitted for clarity. (bottom) View of the *bc* plane of **2** showing the undulating arrangement of the chains. The ORTEP drawing and symmetry operations are given in Figure S3 in the Supporting Information.

Table 3. Cu···Cu Distances (Å) in **2** Recorded at Different Temperatures

Cu···Cu	115 K	173 K	195 K	235 K
Cu1···Cu2	2.7187(9)	2.7309(5)	2.7319(12)	2.7489(9)
Cu2···Cu2#1	2.9904(11)	3.0124(8)	3.0195(17)	3.0373(13)
Cu3···Cu3#2	3.0502(10)	3.0454(7)	3.0446(15)	3.0302(11)

opened tetramer[31,39] and the open-cubane tetramer[22b] depicted in Scheme 1.[40] To the best of our knowledge, no example of a closed-cubane $Cu_4Br_4S_4$ cluster has been structurally characterized, whereas numerous $Cu_4Br_4L_4$ compounds (L = N, P, As, or olefin) are documented in the literature.[41−43]

It is well-known that the choice of the reaction medium may have a crucial impact on the architecture and composition of CuX·thioether adducts.[44,45] For example, the treatment of $[Cu(CO)Cl]_n$ with THT in MeOH, THF, CH_2Cl_2, and dimethoxyethane leads to the formation of $[(CuCl)_2(THT)_3]_n$, $[(CuCl)(THT)]_n$, $[(CuCl)(THT)]_n$, and $[(CuCl)_3(THT)_2]_n$, respectively.[44] In order to exclude any possible solvent impact on the composition of **2** with its 3:3 ligand-to-Cu ratio (instead of the claimed 3:4 ligand-to-Cu ratio), we conducted the reaction between CuBr and excess of SEt_2 in both MeCN and MeOH as the reaction medium. In both cases, the isolated colorless crystals were subjected to a single-crystal analysis. The unit cell parameters of the products issued from crystallization in MeCN and MeOH displayed parameters identical with each other and identical with those obtained for the product crystallized from heptane. Thus, this is ruling out any solvent influence on the formation of **2**. We also tried to grow crystals of a $CuCl\cdot SEt_2$ adduct to unambiguously confirm the $[(Et_2S)_3\{Cu_4(\mu_3\text{-}Cl)_4\}]_n$ formula as previously suggested,[26,46] but no X-ray-quality crystals using a concentrated MeCN solution were obtained.

3. Photophysical Properties and DFT and TDDFT Calculations. 3.1. Photophysical Data of 1. The very intense luminescence observed for polymer **1** under a simple hand-held UV lamp motivated us to investigate in more detail its photophysical properties (Figure S5 in the Supporting Information).

(39) Wang, Y.; Hu, M.-C.; Zhai, Q.-G.; Li, S.-N.; Jiang, Y.-C.; Ji, W.-J. *Inorg. Chem. Commun.* **2009**, *12*, 281–285.
(40) Concerning another partially opened cubane Cu_4Br_4 motif, see: Xue, X.; Wang, X.-S.; Xiong, R.-G.; You, X.-Z.; Abrahams, B. F.; Che, C.-M.; Ju, H.-X. *Angew. Chem., Int. Ed.* **2002**, *41*, 2944–2946.
(41) Goel, R. G.; Beauchamp, A. L. *Inorg. Chem.* **1983**, *22*, 395–400.
(42) Dyason, J. C.; Healy, P. C.; Engelhardt, L. M.; Pakawatchai, C.; Patrick, V. A.; Raston, C. L.; White, A. H. *J. Chem. Soc., Dalton Trans.* **1985**, 831–838. (b) Bowmaker, G. A.; Effendy; Hart, R. D.; Kildea, J. D.; White, A. H. *Aust. J. Chem.* **1997**, *50*, 653–670.
(43) Haakansson, M.; Jagner, S.; Clot, E.; Eisenstein, O. *Inorg. Chem.* **1992**, *31*, 5389–5394.
(44) Solari, E.; Angelis, S. D.; Latronico, M.; Floriani, C.; Chiesi-Villa, A.; Rizzoli, C. *J. Cluster Sci.* **1996**, *7*, 553–566.
(45) Peng, R.; Deng, S.-R.; Li, M.; Li, D.; Li, Z.-Y. *CrystEngComm* **2008**, *10*, 590–597.
(46) The isomerization of dichlorobutenes in the presence of $[(Et_2S)_3\{Cu_4(\mu_3\text{-}Cl)_4\}]_n$ has been investigated. Rostovshchikova, T. N.; Smirnov, V. V.; Kharitonov, D. N.; Rybakov, V. B. *Russ. Chem. Bull.* **1997**, *46*, 1736–1740.

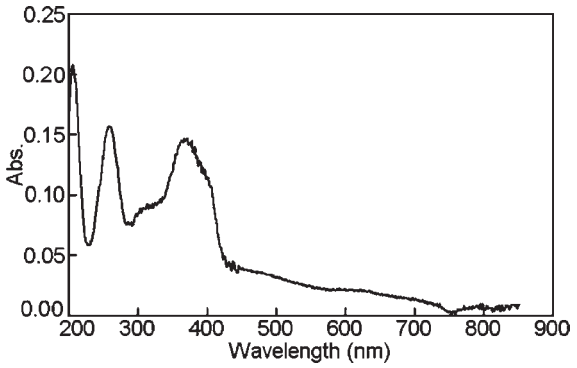

Figure 3. Solid-state absorption spectrum (measured from reflectance) at 298 K of polymer **1**.

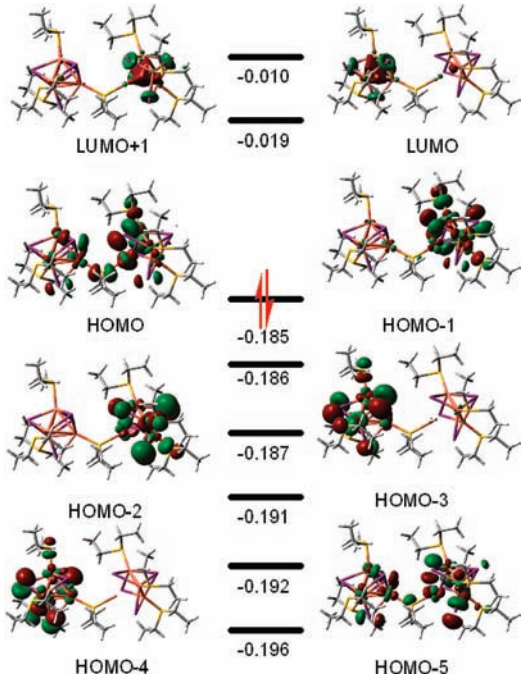

Figure 4. MO diagram for $[Cu_4I_4(SEt_2)_3]_2(\mu\text{-}SEt_2)]$ as a model for the $[Cu_4I_4(SEt_2)_2(\mu\text{-}SEt_2)]_n$ polymer showing the MO pictures going from HOMO−5 to LUMO+1. The units are in atomic units (au).

a. Absorption Spectra. The solid-state absorption spectrum at 298 K of polymer **1** exhibits a series of peaks located at 210, 270, 320, 380, and 400 nm (Figure 3).

Their interpretation was made with the aid of TDDFT using the X-ray structure containing two dissymmetric Cu_4I_4 units bearing four terminal SEt_2 ligands and one SEt_2 bridge for the construction of the input file. The molecular orbital (MO) diagram was generated using this same input file and calculated by DFT. These computed MOs exhibit a rather complex atomic distribution (Figure 4), but the occupied ones (HOMOs) are primarily composed of different combinations of the p orbitals of the S and I (major) atoms and Cu d orbitals. A previously reported study on a related Cu_4I_4-containing dithioether polymer from our groups provided a qualitative description of the frontier MOs.[25b]

The conclusions are similar, and a full description of these MOs does not appear relevant for the purpose of this work. The main feature is that the HOMO-x (x = 0−5) are localized mostly over the whole $Cu_4I_4S_4$ skeleton, whereas the lowest unoccupied MO (LUMO) and LUMO+1 (relevant for the work) are predicted to be mostly localized over the four Cu p orbitals, with some minor contributions of the I lone pairs. Hence, the lowest-energy electronic transitions are mostly cluster-centered (cluster = Cu_4I_4).

Table 4. Computed Transition Energies, Oscillator Strengths, and Major Electronic Contributions for the Six Lowest-Energy Singlet−Singlet Transitions for $[Cu_4I_4(SEt_2)_3]_2(\mu\text{-}SEt_2)]$[a]

wavelength (nm)	f	major contributions (probability in brackets)
343.9	0.028	HOMO−2 → LUMO (30%), HOMO−1 → LUMO (35%), HOMO → LUMO (10%)
335.5	0.010	HOMO−4 → LUMO (72%)
330.3	0.005	HOMO−2 → LUMO (−11%), HOMO → LUMO (61%)
326.0	0.003	HOMO−2 → LUMO (−36%), HOMO−1 → LUMO (42%)
320.5	0.007	HOMO−12 → LUMO (12%), HOMO−7 → LUMO (11%)
315.7	0.019	HOMO−12 → LUMO (−15%), HOMO−2 → LUMO+1 (13%), HOMO−1 → LUMO+1 (17%), HOMO → LUMO+1 (13%)

[a] Only the major contributions are listed. f = oscillator strength.

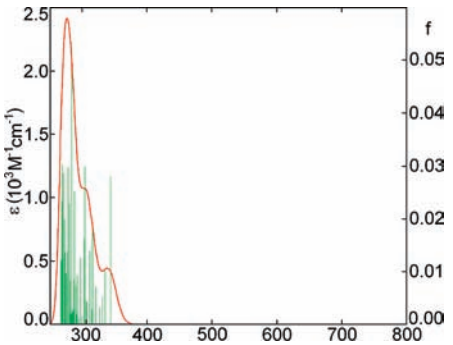

Figure 5. 40 first computed transition positions (in green) and the corresponding absorption spectrum (in red) of the $[Cu_4I_4(SEt_2)_3]_2(\mu\text{-}SEt_2)$ model plotted against the calculated oscillator strength f and absorptivity.

Using TDDFT and the same $[Cu_4I_4(SEt_2)_3]_2(\mu\text{-}SEt_2)]$ model for the $[Cu_4I_4(SEt_2)_2(\mu\text{-}SEt_2)]_n$ polymer, the first 40 spin-allowed singlet−singlet electronic transitions were computed. Table 4 presents the results for the first six transitions as examples in which the wavelength positions, oscillator strengths, and major contributions to the transitions are given. A graph of these first 40 transitions as a function of the wavelength (in green) and generated absorption spectrum (in red) is provided in Figure 5. The last transition is placed at 267.5 nm so the region below this value is not investigated (so there is a cutoff in the calculated spectrum in red at 267 nm). A comparison of the computed (Figure 5) and experimental (Figure 3) spectra shows an agreement for the peak at 270 nm and the weaker features at 300 and 340 nm (corresponding to a broad shoulder at 320 nm in Figure 3). The experimentally observed feature at 380 nm (Figure 3) is assigned to a singlet−triplet transition. It is assumed to be enhanced because the Beer−Lambert law is not linear in the solid state, and so the relative intensity between weak and strong bands can be grossly distorted. Such phenomena are not unusual for solid-state samples and polymers.[47]

(47) Peiponen, K.-E.; Saarinen, J. J. *Rep. Prog. Phys.* **2009**, *72*, 056401/1–056401/19.

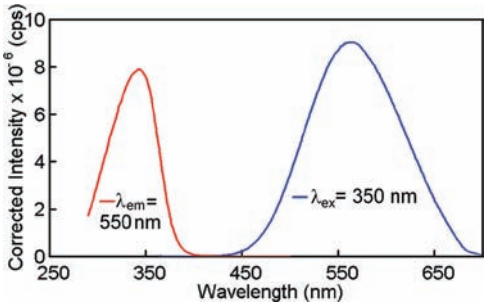

Figure 6. Solid-state emission (blue) and excitation (red) spectra of polymer **1** at 298 K.

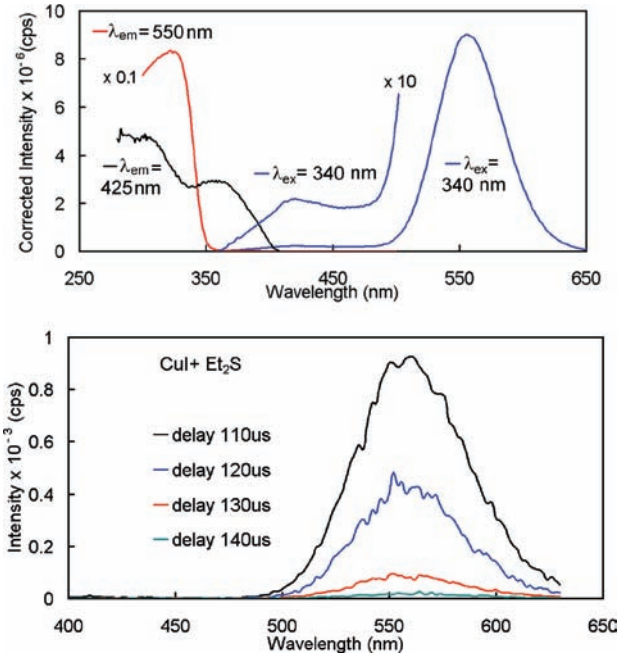

Figure 7. (Top) Solid-state emission (blue) and excitation (red) spectra of polymer **1** at 77 K. (Bottom) Time-resolved emission spectra of the $[Cu_4I_4(SEt_2)_2(\mu\text{-}SEt_2)]_n$ polymer in the solid state at 77 K for various delay times after the laser pulse.

b. Luminescence Spectra. The solid-state emission spectrum of polymer **1** at 298 K is shown in Figure 6.

It exhibits an intense and broad luminescence centered at ~565 nm and a broad excitation band at 340−350 nm. The latter feature matches the low-energy absorption band, both calculated (340 nm) and experimental (broad 320 nm). The energy shift between absorption (or excitation) and emission, combined with the long-lived excited-state lifetime (microsecond time scale) deduced from time-resolved spectra (Figure 7, bottom graph, 77 K data), indicates that the luminescence is a phosphorescence.[39,48]

At 77 K, the emission band of the polymer becomes more intense and sharpens (Figure 7, blue trace) and the excitation band resembles that of 298 K. However, a very weak feature at ~420 nm now appears (black trace) but exhibits an excitation spectrum that differs from the other one. Indeed, the excitation spectrum of this new feature exhibits maxima at 305 and 350 nm. In a previous investigation reported by Kim et al., for a polymer containing the cubane Cu_4I_4 unit and

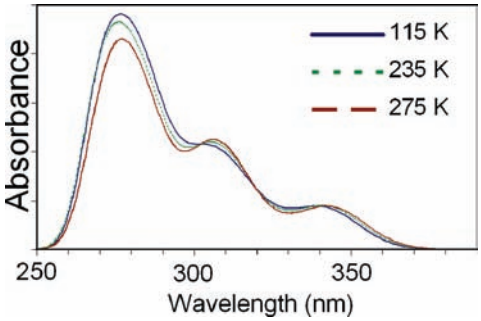

Figure 8. TDDFT-calculated absorption spectra of a $[Cu_4I_4(SEt_2)_3]_2(\mu\text{-}SEt_2)]$ fragment from polymer **1** at three different measured geometries at 115, 235, and 275 K.

dithioether ligand $(PhCH_2SCH_2CH_2OCH_2)_2$ (**L2**), formulated as $[Cu_4I_4(\mathbf{L2})_2]_n$, the same behavior was noted.[49] The authors attributed this upper-energy feature to a cluster-centered excited state (^{3}CC*) mixed with XMCT, consistent with an earlier work reported by Ford and his collaborators.[13b,c] However, one major difference between Kim's work and ours is that they observed a strong red shift of ~55 nm (i.e., 1600 cm^{-1}) but with no apparent change in the fwhm upon cooling from 298 to 7 K. In our work, no apparent shift is observed at all (but a large change in the fwhm is noticed).

This difference between Kim's study on $[Cu_4I_4(\mathbf{L2})_2]_n$[49] and ours was tentatively addressed by computing the absorption spectra of **1** at different temperatures using the X-ray files in the same manner as that described above. Figure 8 compares the calculated absorption spectra of the $[Cu_4I_4(SEt_2)_3]_2(\mu\text{-}SEt_2)]$ fragment for three different temperatures. A slight sharpening is observed, but clearly a modest red shift is computed [on the order of 5−7 nm (i.e., 5 nm = 425 cm^{-1} in this spectral region of 345 nm)]. This is due to the very modest change in Cu···Cu distances in the X-ray structure discussed above (i.e., the Cu···Cu separations decrease very modestly with cooling of the crystals). By assuming that the modest structural ground-state perturbation is transferable from the singlet S_0 manifold to the triplet T_1 manifold, one can easily anticipate that the emission band would also modestly red shift, perhaps by at least 425 cm^{-1} (from 565 nm down to 579 nm; i.e., a ~14 nm shift upon cooling between 275 and 115 K). However, again this shift was not observed (in the 298−77 K window).

The temperature dependence of the emission maximum is not observed for **1**, in spite of similar temperature evolution of the main individual Cu···Cu features (shortening by some 0.05 Å; Table 2) within the Cu_4I_4 SBUs discussed above. In fact, we have the variable-temperature crystal structures for three complexes with Cu_4I_4 SBUs (**1**, solvated, and solvent-free forms of $[Cu_4I_4L_2]_n$ from Kim's group) that show the following features: (i) similar shortening of mean Cu···Cu distances on cooling (0.04, 0.04, and 0.03 Å, respectively), (ii) similar shortening of long Cu···Cu distances (ca. 0.05 Å), (iii) 3.4, 3.2, and 2.2% contraction of the unit cell volume, (iv) mean Cu····Cu distances of 2.794(1), 2.757(3), and 2.729(2) Å at room temperature, (v) mean Cu···Cu distances of 2.756(1), 2.717(1), and 2.701(1) Å at low temperature, and (vi) no shift and 12 and 60 nm red shifts in the emission spectra, respectively.

(48) Lee, J. Y.; Kim, H. J.; Jung, J. H.; Sim, W.; Lee, S. S. *J. Am. Chem. Soc.* **2008**, *130*, 13838–13839.

(49) Kim, T. H.; Lee, K. Y.; Shin, Y. W.; Moon, S.-T.; Park, K.-M.; Kim, J. S.; Kang, Y. *Inorg. Chem. Commun.* **2005**, *8*, 27–30.

Table 5. Temperature Dependence of the fwhm for Different $[Cu_4I_4(thioether)]_n$ Polymers

	298 K		77 K		
polymer[a]	fwhm (nm)	fwhm (cm^{-1})	fwhm (nm)	fwhm (cm^{-1})	Δ (cm^{-1}),[b] ref
$[Cu_4I_4(SEt_2)_2$-$(\mu$-$SEt_2)]_n$	117	3680	60	1900	1780, this work
$[Cu_4I_4(PhS$-$(CH_2)_4SPh)]_n$	115	3460	76	2110	1350, 25b
$[Cu_4I_4(\mathbf{L1})_2]_n$	76	2820	57	1980	840, 32
$[Cu_4I_4(\mathbf{L2})_2]_n$	99	3140	93	2560	580, 49

[a] **L1** = 2-(cyclohexylthio)-1-thiomorpholinoethanone and **L2** = $(PhCH_2SCH_2CH_2OCH_2)_2$. [b] Δ = fwhm(298 K) − fwhm(77 K). The uncertainties on the fwhm are ±50 cm^{-1}.

A careful re-examination of the emission bands at 298 and 77 K (Figures 6 and 7) shows a clear difference in the fwhm (117 ± 2 nm = 3680 cm^{-1} vs 60 ± 2 nm = 1900 cm^{-1}, respectively). This means that the origin of the unresolved vibronic progression (0−0) must be placed at a longer wavelength for the 77 K spectrum, which is totally consistent with the decrease in the Cu···Cu separation with the temperature. In fact, a comparison of the "start" on the short-wavelength side of the emission band suggests that a 0−0 origin may very likely be at ~500 and ~450 nm for the 298 and 77 K spectra, respectively. The exact value for this red shift will probably never be known at these temperatures. Nonetheless, there is indeed a red shift, but it is compensated for by a large change in the fwhm, a change that was not obvious in Kim's work.

One can ask the question, why there is a large change in the fwhm in **1** with the temperature but not or very little for Kim's polymer ($[Cu_4I_4(\mathbf{L2})_2]_n$?[49] The answer likely lies in a difference in the bridging ligand rigidity [Et_2S vs $(PhCH_2SCH_2CH_2OCH_2)_2$]. Upon cooling, a flexible ligand would allow excited-state distortion (structural changes in the excited states) to occur more easily (a large excited-state distortion leads to a broad absorption or emission band, whereas a small excited-state distortion leads to a narrower band). Conversely, a rigid ligand would be less prone to adapt to the excited-state distortion. So, upon cooling, the medium becomes more rigid and an already rigid polymer would be trapped in an even more rigid environment. So, large excited-state distortions are somewhat precluded, hence explaining the narrower emission for **1**. A similar situation was also recently observed by our group,[25b] where the use of a more rigid ligand [$PhSCH_2C{\equiv}CCH_2SPh$ vs $PhS(CH_2)_4SPh$] not only produced different clusters (Cu_6I_6 vs Cu_4I_4, where the Cu···Cu separations are longer for the Cu_6I_6 species) but also induced emission spectra, where the largest change in the fwhm (between 298 and 77 K) is larger for the polymer using the more rigid ligand ($PhSCH_2C{\equiv}CCH_2SPh$). Table 5 compares the fwhm values for four $[Cu_4I_4(thioether)]_n$ polymers. The trend between bridging ligand flexibility and the change in the fwhm on the emission bands with the temperature is indeed qualitatively observed.

Moreover, Coppens and collaborators reported the time-resolved single-crystal diffraction at 17 K of a trimeric species ([3,5-$(CF_3)_2$pyrazolate]Cu)$_3$ upon excitation at 355 nm.[50] The intermolecular Cu···Cu separations contract by 0.56 Å on going from 4.018(1) (ground state) to 3.46(1) Å (excited state; excimer), and the intramolecular contacts shorten by 0.65 Å (ground state) on going from 3.952(1) to 3.33(1) Å (excited state; excimer). Although the nature of the species compared (ground state vs excimer) does not exhibit identical electronic structures, the concept of long separations giving rise to more variation in the Cu···Cu distances upon stimuli (here UV excitation) is also observed. One may argue that the longer intermolecular Cu···Cu separations should have varied more, but again the electronic structures of the ground- and excited-state species are different.

(50) Vorontsov, I. I.; Kovalensky, A. Y.; Chen, Y.-S.; Graber, T.; Gembicky, M.; Novozhilova, I. V.; Omary, M. A.; Coppens, P. *Phys. Rev. Lett.* **2005**, *94*, 19003-1–193003-4.

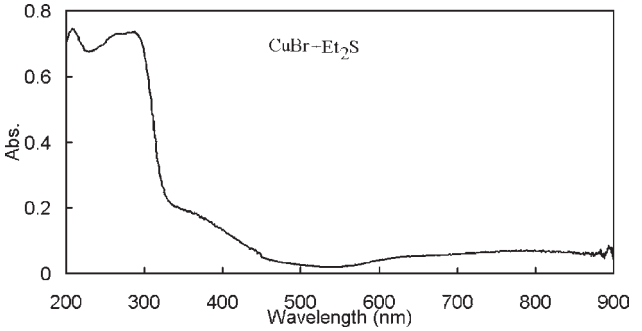

Figure 9. Solid-state absorption spectrum (measured from reflectance) at 298 K of polymer **2**.

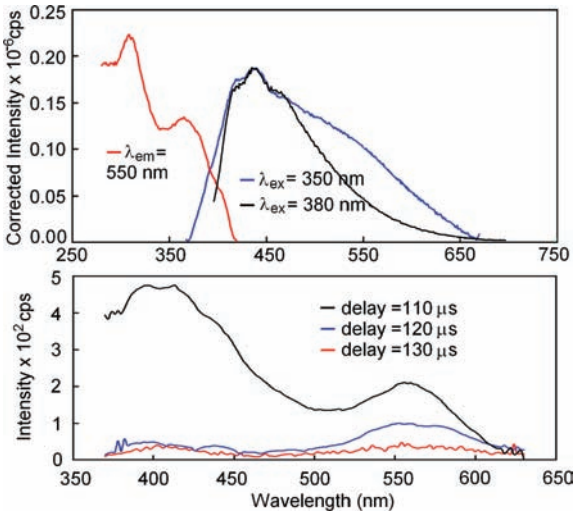

Figure 10. (Top) Solid-state emission (blue) and excitation (red) spectra of polymer **2** at 77 K. (Bottom) Time-resolved emission spectra of polymer **2** in the solid state at 298 K for various delay times after the laser pulse with λ_{ex} = 350 nm.

3.2. Photophysical Data of 2. a. Absorption Spectra. The solid-state electronic spectrum (Figure 9) at 298 K of polymer **2** exhibits absorption features at 210, 270, 290, and 365 nm (broad shoulder). It is clearly different from that of polymer **1**.

b. Luminescence Spectra. The solid-state emission spectra of **2** at 77 K (Figure 10) and 298 K are very similar, where two emissions are depicted at 440 (weakly resolved) and 550 nm (shoulder). The 440 nm feature bears resemblance to that observed at 430 nm for polymer **1** (Figure 7) and may again be due to a different upper excited state. However, the broad and long-lived 550 nm band, which can be resolved from time-resolved spectroscopy, is more

Table 6. Emission Lifetimes of Polymers **1** and **2**

	298 K		77 K	
	λ_{em} (nm)	τ (μs) or λ_{em} (nm)	λ_{em} (nm)	τ (μs) or λ_{em} (nm)
$[Cu_4I_4(SEt_2)_2(\mu\text{-}SEt_2)]_n$ (**1**)			425	0.89 ± 0.02
	565	7.34 ± 0.05	565	8.8 ± 0.06
$[Cu_3Br_3(SEt_2)_3]_n$ (**2**)	425	0.89 ± 0.01	440	2.53 ± 0.05
	550	0.78 ± 0.01	550	1.47 ± 0.02

difficult to assign because of the presence of two chromophores in the backbone of the polymer (i.e., Cu_2Br_2 and Cu_4Br_4). The Cu_4I_4 emission observed at 565 nm in the more symmetric unit of polymer **1** is close to that observed at 550 nm for the open-cubane Cu_4Br_4 cluster-containing polymer **2**.

The emission lifetimes have also been measured for characterization purposes (Table 6). There is an increase in the emission lifetimes of the 565 and 550 nm bands upon cooling of the samples. This increase in the lifetimes is consistent with a decrease of the nonradiative rate constant, k_{nr}, upon cooling. This could be associated with an increase in the medium rigidity upon solid-state contraction visible in the unit cell parameter shortenings. Moreover, the data indicate that the emission lifetime for the 550 nm luminescence (i.e., arising from the open-cubane Cu_4Br_4 unit of the $[Cu_3Br_3(SEt_2)_3]_n$ polymer) is shorter than that for the 565 nm emission of the cubane-like Cu_4I_4 fragment of the $[Cu_4I_4(SEt_2)_2(\mu\text{-}SEt_2)]_n$ polymer. This observation suggests that the open-cubane structure is more flexible than the rigid cubane, hence providing more pathways for nonradiative deactivation. This comparison neglects the electronic effects caused by the halides, but the closed-cubane Cu_4Br_4 cluster and the open-cubane Cu_4I_4 unit have not been observed so far.

4. Conclusion and Perspectives. This work has addressed the true nature of an old coordination polymer, **2**, previously reported to be "$[Cu_4Br_4(SEt_2)_3]_n$" and believed to be isostructural to **1** solely on the basis of elemental analysis. However, despite trying different experimental conditions, namely, different solvents, the X-ray structure revealed only one form for **2** ($[Cu_3Br_3(SEt_2)_3]_n$). Very interestingly, the obtained coordination polymer exhibits a 1D chain using two types of repetitive clusters, Cu_4Br_4 and Cu_2Br_2.

It is worth noting that the luminescence arising from clusters of the type $Cu_4Br_4S_4$ and $Cu_2Br_2S_4$ (S = thioether) was unknown so far. Ideally, a comparison should be made with similar species (i.e., Cu_4I_4 with Cu_2I_2; Cu_4Br_4 with Cu_2Br_2). Fortunately, the change in the halide (X = Cl, Br, I) does not drastically change the emission maxima of the $Cu_4X_4L_4$ clusters (L = N and P donors).[13c] Variable-temperature experiments demonstrated that the X-ray Cu···Cu distance slightly shortens upon cooling but, unexpectedly, the emission maximum (565 nm) did not for polymer **1**. Conversely, the fwhm decreased dramatically, which leads to the spectroscopic conclusion that the vibronic origin of the emission band (although not resolved in this work) red shifts, as it was originally anticipated based upon previous literature data but also based upon the calculated absorption spectra at different temperatures by TDDFT. A comparison of the change in the fwhm of the emission band of **1** and three other literature Cu_4I_4(dithioether)$_2$-containing coordination polymers (noted as Δ in Table 5; four entries) with the temperature between 298 and 77 K follows a trend. Indeed, Δ becomes smaller as the bridging ligand becomes more flexible. This observation is tentatively explained by the relative ease of the $Cu_4I_4S_4$ chromophore to undergo excited-state distortion as a function of the medium rigidity.

We also noted that the overall luminescence behavior (emission maximum and lifetime) of polymer **1** resembles somewhat that for the recently reported $[Cu_4I_4(PhS(CH_2)_4SPh)_2]_n$, except that a temperature dependence of the emission maximum between 298 and 77 K is observed for the latter polymer, and that the XMCT emission band is more visible for polymers **1** and **2** in comparison with that of $[Cu_4I_4(PhS(CH_2)_4SPh)_2]_n$.[25b] It becomes apparent that a comparison of a large number of polymers and discrete compounds of this family may shine some light on why this upper-energy XMCT luminescence is often intense with respect to lower-energy ^{3}CC* emission. In other words, what are the structural parameters that control the excited-state dynamics that regulate the emission properties of these two emissive states?

Future work involves DFT/TDDFT analysis of the luminescent "simple" discrete molecules $[Cu_4I_4(SPr_2)_4]$ and $[Cu_2Br_2(p\text{-}TolSCH_2CH_2STol\text{-}p)_4]$ (recently obtained) and $[Cu_2I_2(THT)_4]$.[29] The nature of the excited states between bi- and tetranuclear clusters will be compared. Moreover, new coordination polymers of the type $[Cu_4I_4(ArS(CH_2)_mSAr)_2]_n$ (Ar = C_6H_5, *o*- and *p*-$CH_3C_6H_4$; $m = 1-8$) are currently under investigation for comparison purposes in order to address the relationship between Δ reported in Table 5 and the relative flexibility of the material. It is anticipated that, as the number of methylene groups increases, the flexibility of the material as well as the predicted trend for Δ increases.

Experimental Section

Diethyl sulfide was commercially purchased from Fluka. Polymer **1** was prepared as described in ref 26 using heptane instead of hexane.

Preparation of Polymer 2. CuBr (1.435 g, 10 mmol) was dissolved in neat Et_2S (5 mL) (exothermic reaction), and the resulting brown-yellow solution was stirred for a further 5 h in a Schlenk tube. Heptane (15 mL) was added in three portions. During the addition of the last portion, precipitation of a small amount of a colorless solid was noticed. The Schlenk tube was set into a refrigerator (2 °C), where large colorless crystals of **2** crystallized overnight. A second crop was also isolated after the filtered solution was kept in a freezer at −20 °C. Overall yield: 73%. Anal. Calcd for $C_{12}H_{30}Br_3Cu_3S_3$ (700.89): C, 20.56; H, 4.32; S, 13.72. Found: C, 20.26; H, 4.15; S, 13.22.

Polymer **2** was also obtained as the sole product (X-ray diffraction and a comparison of the luminescence spectra) when CuBr was treated with an excess of Et_2S in a MeOH or MeCN solution.

Instruments. Solid-state UV−vis spectra were recorded on a Varian Cary 50 spectrophotometer. Emission and excitation spectra were obtained by using a double-monochromator Fluorolog 2 instrument from Spex. Phosphorescence lifetimes were measured on a Timemaster model TM-3/2003 apparatus from PTI. The source was a N_2 laser equipped with a high-resolution dye laser (fwhm ~ 1500 ps), and the phosphorescence lifetimes were obtained from deconvolution and distribution lifetime analysis. The excitation wavelength was the primary 337.1 nm line of the N_2 laser.

Crystal Structure Determinations. A prism-shaped colorless single crystal of **1** was mounted on a Nonius Kappa Apex-II

CCD diffractometer equipped with a N_2 jet stream, low-temperature system (Oxford Cryosystems). The X-ray source was graphite-monochromated Mo Kα radiation (λ = 0.710 73 Å) from a sealed tube. The lattice parameters were obtained by a least-squares fit to the optimized setting angles of the entire set of collected reflections. Intensity data were recorded as ϕ and ω scans with κ offsets. No significant intensity decay or temperature drift was observed during data collection. Data were reduced by using *DENZO* software[51] without applying absorption corrections; the missing absorption corrections were partially compensated for by the data-scaling procedure in the data reduction. Absorption corrections were applied by using *MULTISCAN*.[52] The structure was solved by direct methods with the *SHELXS97* program.[53] Refinements were carried out by full-matrix least squares on F^2 using the *SHELXL97* program on the complete set of reflections.[53] All non-H atoms were refined with anisotropic thermal parameters. The H atoms were placed in calculated positions and included in the final refinement in a riding model with the isotropic temperature parameters set to $U_{iso}(H) = 1.2U_{eq}(CH_2)$ and $U_{iso}(H) = 1.5U_{eq}(CH_3)$.

The same crystallographic protocol was employed for the treatment of one selected crystal of **2** at three different temperatures (115, 195, and 235 K). A second colorless single crystal of **2** was mounted on a Bruker APEX diffractometer (D8 three-circle goniometer; Bruker AXS) equipped with a self-build N_2 stream, low-temperature system. The lattice parameters were obtained by a least-squares fit to the optimized setting angles of the entire set of collected reflections. Intensity data were recorded at 173 K. No significant intensity decay or temperature drift was observed during data collection. Data were reduced by using *SMART*, version 5.622 (Bruker AXS, 2001), software, by applying an absorption correction with *SADABS*, version 2.01 (Bruker AXS, 1999). The structure was solved by direct methods with the *SHELXS97* program.[53] Refinements were carried out by full-matrix least squares on F^2 using the *SHELXL97* program.[53] All non-H atoms were refined with anisotropic thermal parameters. The H atoms were placed in calculated positions and included in the final refinement in a riding model with the isotropic temperature parameters set to $U_{iso}(H) = 1.2U_{eq}(CH_2)$ and $U_{iso}(H) = 1.5U_{eq}(CH_3)$.

Computational Details. Calculations were performed with *Gaussian 03*[54] at Université de Sherbrooke on the Mammouth MP supercomputer supported by le Réseau Québécois de Calculs de Haute Performances. The DFT[55−57] and TD-DFT[58−60] were calculated with the B3LYP[61−63] method. 3-21G*[64] basis sets were used for C and H and SBKJC-polarized (p, 2d) basis sets for S and I,[65] and the SBKJC basis set with effective core potentials was used for Cu.[64a,66] The calculated absorption spectra and related MO contributions were obtained from the TDDFT output file and *gausssum2.1*.[67]

Acknowledgment. P.D.H. thanks the Natural Sciences and Engineering Research Council of Canada, Fonds Québécois de la Recherche sur la Nature et la Technologie, and Centre d'Études des Matériaux Optiques et Photoniques de l'Université de Sherbrooke for funding. M.K., M.M.K., and C.S. thank the CNRS, DFG, and Centre de Coopération Universitaire Franco-Bavarois for financial support.

Supporting Information Available: X-ray crystallographic data in CIF format, ORTEP views of polymers **1** and **2**, packing diagram of **1** and a perspective view of **2** down the *c* axis, and photographs showing the solid-state luminescence of **1** and $[(THT)_2Cu(\mu_2\text{-}I)_2Cu(THT)_2]$. This material is available free of charge via the Internet at http://pubs.acs.org.

(51) Otwinowski, Z.; Minor, W. *Methods Enzymol*. **1997**, *276*, 307–326.
(52) Blessing, R. H. *Acta Crystallogr*. **1995**, *A51*, 33–38.
(53) Sheldrick, G. M. *SHELXS97 and SHELXL97; Programs for the Solution and Refinement of Crystal Structures*; University of Göttingen: Göttingen, Germany, **1997**.
(54) *Gaussian 03*, revision C.2; Gaussian, Inc.: Wallingford, CT, **2004**.
(55) (a) Hohenberg, P.; Kohn, W. *Phys. Rev*. **1964**, *136*, B864–B871. (b) Kohn, W.; Sham, L. J. *Phys. Rev*. **1965**, *140*, A1133–A1138.
(56) Salahub, D. R.; Zerner, M. C. *The Challenge of d and f Electrons*; American Chemical Society: Washington, DC, 1989.
(57) Parr, R. G.; Yang, W. *Density-functional theory of atoms and molecules*; Oxford University Press: Oxford, U.K., 1989.
(58) Stratmann, R. E.; Scuseria, G. E.; Frisch, M. J. *J. Chem. Phys*. **1998**, *109*, 8218–8224.
(59) Bauernschmitt, R.; Ahlrichs, R. *Chem. Phys. Lett*. **1996**, *256*, 454–464.
(60) Casida, M. E.; Jamorski, C.; Casida, K. C.; Salahub, D. R. *J. Chem. Phys*. **1998**, *108*, 4439–4449.
(61) Becke, A. D. *J. Chem. Phys*. **1993**, *98*, 5648–5652.
(62) Lee, C.; Yang, W.; Parr, R. G. *Phys. Rev. B: Condens. Matter Mater. Phys*. **1988**, 785–789.
(63) Miehlich, B.; Savin, A.; Stoll, H.; Preuss, H. *Chem. Phys. Lett*. **1989**, *157*, 200–206.
(64) (a) Binkley, J. S.; Pople, J. A.; Hehre, W. J. *J. Am. Chem. Soc*. **1980**, *102*, 939–947. (b) Gordon, M. S.; Binkley, J. S.; Pople, J. A.; Pietro, W. J.; Hehre, W. J. *J. Am. Chem. Soc*. **1982**, *104*, 2797–2803. (c) Pietro, W. J.; Francl, M. M.; Hehre, W. J.; Defrees, D. J.; Pople, J. A.; Binkley, J. S. *J. Am. Chem. Soc*. **1982**, *104*, 5039–5048. (d) Dobbs, K. D.; Hehre, W. J. *J. Comput. Chem*. **1986**, *7*, 359–378. (e) Dobbs, K. D.; Hehre, W. J. *J. Comput. Chem*. **1987**, *8*, 861–879. (f) Dobbs, K. D.; Hehre, W. J. *J. Comput. Chem*. **1987**, *8*, 880–893.
(65) (a) Labello, N. P.; Ferreira, A. M.; Kurtz, H. A. *J. Comput. Chem*. **2005**, *26*, 1464–1471. (b) Labello, N. P.; Ferreira, A. M.; Kurtz, H. A. *Int. J. Quantum Chem*. **2006**, *106*, 3140–3148.
(66) (a) Stevens, W. J.; Basch, H.; Krauss, M. *J. Chem. Phys*. **1984**, *81*, 6026–6033. (b) Stevens, W. J.; Krauss, M.; Basch, H.; Jasien, P. G. *Can. J. Chem*. **1992**, *70*, 612–630. (c) Cundari, T. R.; Stevens, W. J. *J. Chem. Phys*. **1993**, *98*, 5555–5565.
(67) O'Boyle, N. M.; Tenderholt, A. L.; Langner, K. M. *J. Comput. Chem*. **2008**, *29*, 839–845.